# The classification of renal stones by gratings-based dark-field radiography

Tilo Niemann[1], Iwan Jerjen[2,3], Lukas Hefermehl[4], Zhentian Wang[2], Rahel A. Kubik-Huch[1], Marco Stampanoni[2,3]

[1]Kantonsspital Baden, Department of Radiology, Baden, Switzerland
[2]ETH Zurich, Department of Information Technology and Electrical Engineering, Zurich, Switzerland
[3]Paul Scherrer Institute, Villigen, Switzerland
[4]Kantonsspital Baden, Department of Urology, Baden, Switzerland

Citation: Niemann T, Jerjen I, Hefermehl L, Wang Z, Kubik-Huch RA, Stampanoni M. The classification of renal stones by gratings-based dark-field radiography. Cent European J Urol. 2021; doi: 10.5173/ceju.2021.3.0334 [Epub ahead of print]

Article history
Submitted: Nov. 18, 2020
Accepted: June 30, 2021
Published online: Sept. 9, 2021

Corresponding author
Tilo Niemann
Kantonsspital Baden
Department of Radiology
1 Im Ergel Street
CH-5404 Baden,
Switzerland
phone: +41 56 486 21 11
tilo.niemann@ksb.ch

**Introduction** Occurrence of urinary calculi is a common medical condition. Since treatment and prevention measures depend on the type of stone found, reliable diagnostic tools are required. Dual energy computed tomography (CT) allows for rough classification of the stones found. After extraction, stone composition can be confirmed by laboratory analysis.
We investigated to which degree gratings-based X-ray interferometry, which can measure attenuation, refraction and scattering (dark-field) properties of samples, allows for the discrimination of urinary stone type by calculating the ratio (R) of attenuation and scattering signals.
**Material and methods** In an experimental setup we investigated 322 renal stone fragments from 96 patients which were extracted during routine clinical practice. Laboratory analysis showed the chemical composition of the urinary stones.
These were correlated with dark field analysis of the stone samples. Measurements were performed on a X-rays gratings interferometer prototype. The attenuation, refraction and scattering signals were measured and the R-value calculated.
**Results** The spread of R-values of a given type of calculi is large, reducing the specificity of the method. Only uric acid stones can reliably be distinguished (sensitivity of 0.86 at a specificity of 0.9) from the other stones.
**Conclusions** Gratings-based dark-field imaging is a non-destructive and potentially non-invasive technique that allows to discriminate between uric acid and non-uric acid stones, which from a clinical point of view represents by far the most important question for stone treatment.

Key Words: urolithiasis ‹› dark field imaging ‹› sensitivity ‹› specificity

## INTRODUCTION

Urinary stone formation is a widespread problem with prevalence rates up to 20% [1]. Particularly in areas with a high standard of life there has been rapid increase of prevalence up to 37% over the last 20 years [2–4].
There is a variety of different stone compositions, such as calcium-oxalate, uric acid, ammonium urate, xanthine, magnesium ammonium phosphate, apatite, cystine and drug-stones.

Stone differentiation is one of the most important corner stones in the diagnostic and treatment pathway of urinary calculi [5]. In case of uric acid stones, for example, non-invasive treatment options, such as pharmacological and dietary measures can lead to complete stone-free status even in patients with a considerable stone load. While shock wave lithotripsy (SWL) can be a potent procedure for many different types of kidney stones, it is often not effective for extremely hard stones such as calcium oxalate monohydrate stones [6, 7]. Hence, in these cases,

laser-lithotripsy during ureterorenoscopy (URS) or percutaneous nephron-litholapaxy (PNL) should be preferred [8]. Furthermore, stone composition is the most important predictor for determining the aetiology of stone formation, and therefore leading to individualized recommendations for stone-prevention. The gold standard for stone differentiation is infrared spectroscopy (IRS) and X-ray diffraction (XRD) [9, 10, 11]. Alternatively, polarisation microscopy can be used, while chemical analysis is considered to be obsolete [9].

Conventional X-ray AC computed tomography (CT) is the method of choice for diagnosing renal colic [1, 4–7]. It allows locating renal stones, depicting complications or detecting alternative pathology [5]. The exact size and type of the stone can be determined [1, 4, 7]. Dual-energy CT improves the quality of the diagnosis considerably. Indeed, the stones can be identified with a high degree of certitude [9]. However, CT is always associated with radiation exposure and therefore induced risks. This should be considered especially in younger patients. Therefore, care has to be taken to "use radiation doses that are as low as reasonably achievable (ALARA)" [10].

In recent years considerable progress in X-ray technology has taken place, leading to an emerging interest for medical imaging applications (e.g. lung, breast) [12, 13, 14]. One of the most promising developments in this area is dark-field X-ray imaging [15–18]. Scherer et al. have reported that X-ray dark-field radiography can be used as a highly specific and sensitive method for stone differentiation. Their study aimed to discriminate between uric acid, calcium oxalate and 'mixed types' only [19, 20].

On the other hand, CT-stone differentiation (e.g. by density in attenuation measurements; dual-energy differentiation) has been proved to be highly specific for uric-acid stones and calcium-oxalate stones, respectively. Approximately one third of all stones are 'mixed types', meaning that the stones are composed of layers of at least two stone types (e.g. calcium oxalate di-hydrate and magnesium ammonium phosphate).

The objective of this study was to investigate if the high sensitivity and specificity of X-ray dark-field imaging for differentiating renal stones reported by Scherer et al. [19] can be confirmed in a data set of consecutive clinical stone samples.

## MATERIAL AND METHODS

### Collection of renal stones

Patients with acute flank pain and suspected renal colic were routinely examined by a standardized low-dose non-contrast dual energy CT protocol (Definition Flash, Siemens, Erlangen Germany) at Kantonsspital Baden, Switzerland. All patients were asked to collect their passed stones. These fragments were analyzed at Paul-Scherrer-Institute by gratings-based dark-field X-ray radiography. Stone composition was determined additionally by laboratory analysis, which was the gold standard.

### Renal stone population

The study was approved by the local ethical commission (EKNZ 2015-00207).

A total of 322 renal stone fragments were included in the analysis from 96 consecutive patients (69 male, 28 female, age 23–87 years) at Kantonsspital Baden during the period from March 2016 to January 2017. The sample population was 104, as this is the number of stones which have been retrieved. The composition (main and secondary components) of the stones was determined with infrared spectroscopy in laboratory analysis. Table 1 lists the inves-

**Table 1.** *Nomenclature, chemical formula, density and relative occurrence of the investigated renal stone components in lab analysis*

| Type | Chemical formula | Density [g/cm³] | Relative occurrence |
|---|---|---|---|
| Whewellite | $Ca(C_2O_4)\cdot H_2O$ | 2.22 | 79% |
| Weddelite | $Ca(C_2O_4)\cdot 2H_2O$ | 1.96 | 32% |
| Apatite | $Ca_5[(F,Cl,OH)\mid(PO_4)_3]$ | 3.2 | 37% |
| Uricite | $C_5H_4N_4O_3$ | 1.85 | 10% |

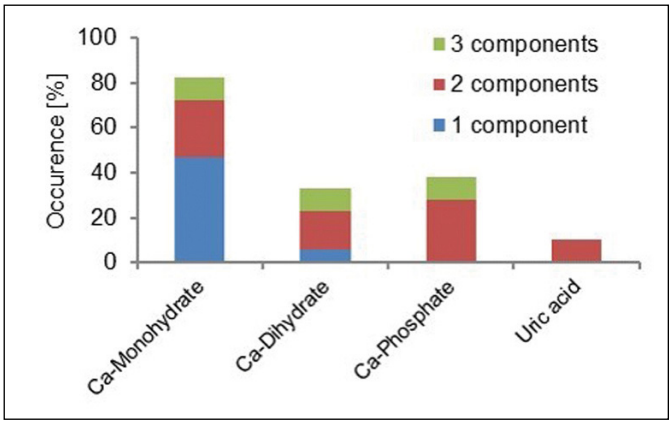


**Figure 1.** *Investigated renal stone population. Stone retrievals with just one component are indicated in blue, stones with 2 or 3 components in red and green, respectively. In total, there were 104 retrievals. Our distribution globally corresponds to the occurrence of stones as presented in the study by Acharya et al. [24].*

tigated stone components, their chemical composition, density and their relative occurrence. In about 79% of retrievals, whewellite was found, in 32% weddelite, in 37% apatite and in 10% uricite.
Figure 1 displays the occurrence of the investigated stone types. In slightly over half of retrievals, only one stone type was found (blue). In about 10% of retrievals, three components were found (green) and in about 40% two components (red) were found.

**Table 2.** *Specification of the components of the dark-field X-ray instrument*

| X-ray detector | | Hamamatsu C9732DK-11 | | |
|---|---|---|---|---|
| Technology | Scintillator | Active area | Pixel size | Dynamic range |
| CMOS | CSI | 120x120 mm$^2$ | 50x50 µm$^2$ | 5100 |
| X-ray tube | | I.A.E. Spa XM15 T | | |
| Technology | Max. voltage | Max. power at 0.1 and 0.4 mm spot size | | X-ray Window |
| Rotating anode | 49 kV | 2 kW | 8 kW | 0.5 mm Be |
| Interferometer | | Manufactured by Microworks | | |
| Gratings | | Period | Thickness | Pitch |
| Au source grating $G_0$ | | 12.113 µm | 50 µm | 0.5 |
| Si phase grating $G_1$ | | 4.811 µm | 1 µm | 0.5 |
| Au analyzer grating $G_2$ | | 3.000 µm | 50 µm | 0.5 |
| Intergrating distances | | $G_0$–$G_1$ 881.9 mm | $G_1$–$G_2$ 218.1 mm | $G_0$–$G_2$ 1100 mm |

## Gratings-based dark-field X-ray radiology

A gratings-based Talbot-Lau interferometer measures attenuation, refraction and scattering of an X-ray beam passing through an object [18]. In conventional radiographic images, the contrast between renal stones and the surrounding tissue depends on the material-specific attenuation coefficient and the X-ray path length. In dark-field radiography, the contrast between materials arises from the scattering coefficient and the X-ray path length. The path length independent R-value is given by the ratio of the absorption vs. the scattering contribution of the sample, the latter is accessed via the measurement of the visibility signals of the Talbot-Lau interferometer [21, 22].
The strength of the attenuation is proportional to the density of a sample and depends strongly on the chemical composition (i.e. atomic number of the elements). The scattering power is very sensitive to the (unresolved) structure within a sample [14, 15], so that differentiation of the stones based on their micro-structure may be achieved through the analysis of the R-values distribution.

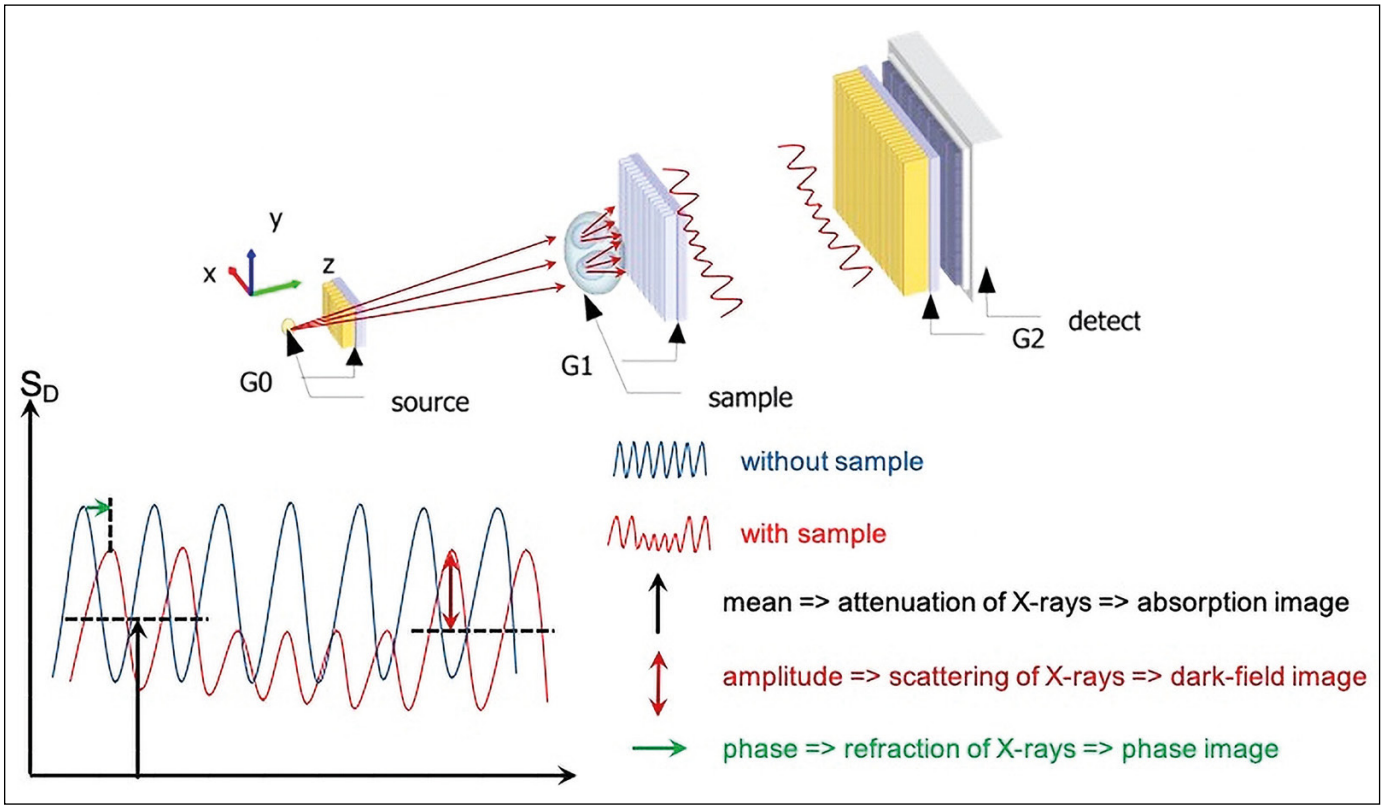


**Figure 2.** *Dark-field imaging (DFI): Talbot-Lau interferometer setup.*

### Gratings-based dark-field X-ray radiography instrument

The dark-field X-ray radiographic measurements were performed on a vertical Talbot-Lau X-ray interferometer constructed at PSI. The vertical setup has a grating interferometer designed for 25 keV and the gratings were manufactured by Microworks (Microworks GmbH, Eggenstein-Leopoldshafen, Germany). The X-ray source is an X-ray tube from I.A.E Spa (XM15 T), and the X-ray detector is a Hamamatsu flat panel (C9732DK-11). The field of view (FOV) of setup is 8 cm x 4 cm, which is limited by the grating size. Figure 2 illustrates the setup of the Talbot-Lau X-ray interferometer.
Table 2 shows the specification of the components of the dark-field X-ray instrument.

### Data analysis

The attenuation, differential phase and scattering signals were obtained by analyzing the interference pattern created by the Talbot-Lau interferometer following the phase stepping procedure as described by Weitkamp et al. [23]. Here, 16 steps were used for obtaining the reference pattern and 8 steps for obtaining the pattern with the samples. The parameters of the sinusoidal curves of the interference patterns were obtained by applying a least square error fit. This avoids the significant error obtained if a Fourier transformation is used for determining the parameters of a sinusoidal curve where the sampling points are not evenly distributed over the exact period of the curve. The quality of the fit was cross-checked by creating a map of the least square error between the fitted and the measured interference patterns.
All stone fragments were measured twice to ensure that at least one measurement was of good quality. The stone fragments were segmented from the background by applying a threshold in the absorption image. After subtracting the background levels (originating from the specimen holder), R -images were calculated.
To improve the differentiation of peaks, each image was filtered (median filter with radius of 5 pixels) before a histogram of the R-values was calculated. The obtained histograms were fitted with a sum of Gaussian peaks to allow more efficient further analysis.
Since in the laboratory analysis, the composition type of urinary stone was determined for a given retrieval which may consist of several stone fragments, the dark-field data of the fragments had to be grouped together. This was done by calculating the weighted mean of all peak positions found in the histograms of all fragments obtained from a given patient.

To test the hypothesis that the stone types can be differentiated by their characteristic R-value, the AUC (area under curve) values of all the ROC (receiver operating characteristic) curves obtained for 100 different R-values evenly distributed between 0 and 1 were calculated for each type of calculi (Figure 3). The R-value which optimizes the ROC curve for a given calculi type is then considered to be specific for this calculi.

## RESULTS

The R-values of some stone fragments of one type/composition differ significantly and some fragments of different types can exhibit similar R-values, they may even show similar R-images. As an example, Figure 4 shows the R-images of four calculi, two Ca-monohydrate stones (a and b) and two uric acid stones (c and d). Clearly, (a) and (c) respectively (b) and (d) have grey values (i.e. R -ignals) closer to each other than to their counterpart.
Nevertheless, optimal R-values for differentiating uric acid, Ca-monohydrate, Ca-dihydrate and Ca-phosphate stones, respectively, were obtained (see Figure 3). Values smaller than 0.15 are ideal for detecting uric acid stones, values higher than 0.6 allow finding Ca-monohydrate stones and an R-value of 0.25 allows identifying both, Ca-dihydrate and Ca-phosphate stones.
Figure 5 shows the ROC curves of the four investigated stone compositions. We deduced that uric acid stones are reliably distinguished from other stones

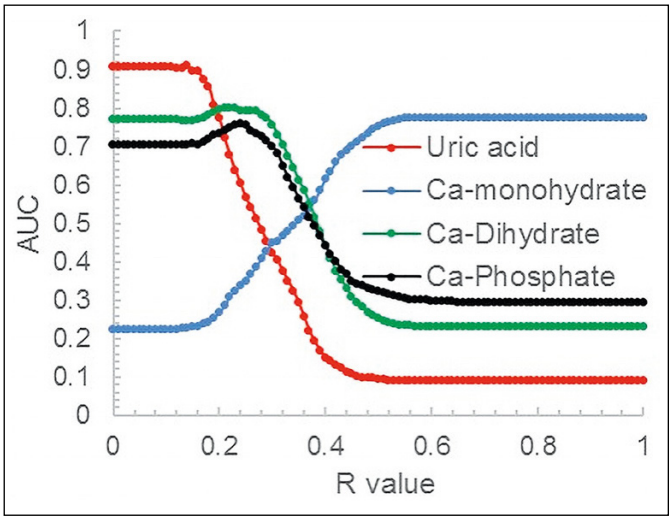


**Figure 3.** *Area under curve (AUC) values of dihydrate and Ca-phosphate stones cannot be distinguished from each other, both have an optimal R-value at approximately 0.25. The uric acid stones have R-values predominantly below 0.15 and the Ca-monohydrate stones of above 0.6.*

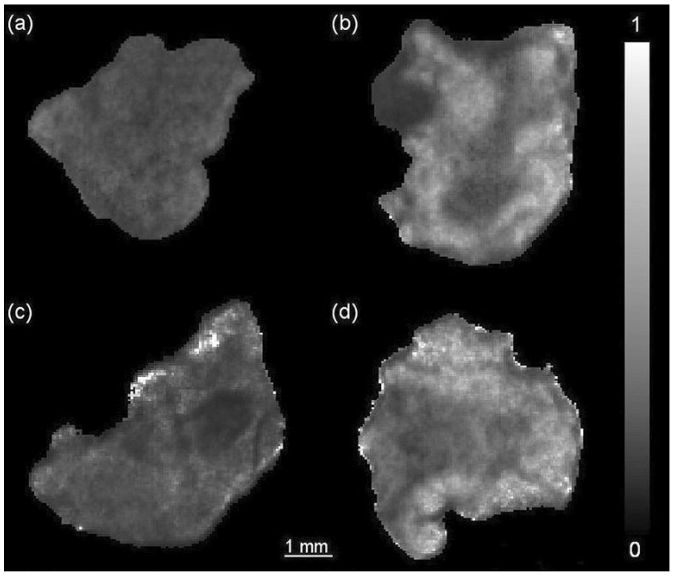


**Figure 4.** *R-images of two Ca-monohydrate calculi (a and b) and two uric acid calculi (c and d). Black and white correspond to R values of 0 and 1, respectively.*

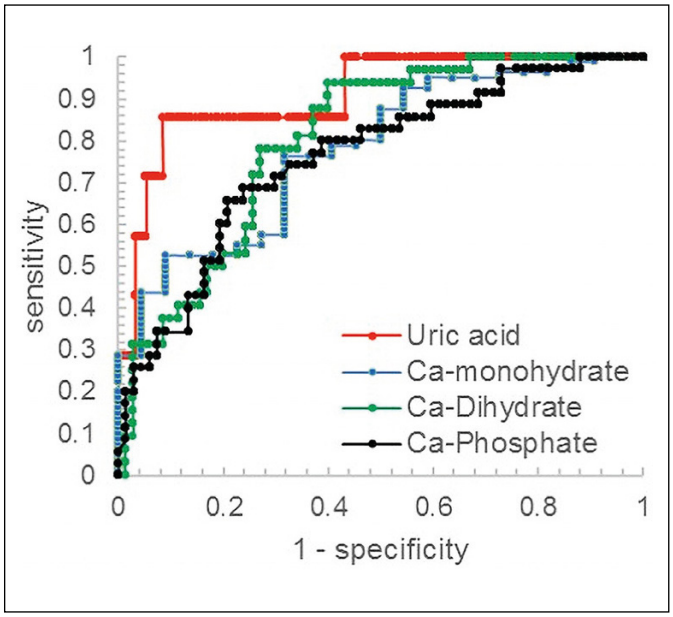


**Figure 5.** *Receiver operating characteristic curves for the four most common calculi: uric acid in red, Ca-monohydrate in blue, Ca-dihydrate in green and Ca-phosphate in green.*

by the R-value. We observed that Ca-monohydrate stones have statistically higher R-values than all the other stones, interestingly also higher than the chemically very similar Ca-dihydrate stones. In our study, Ca-phosphate stones showed the same R-value as the Ca-dihydrate stones. The area under curve (AUC) values for uric acid, Ca-monohydrate, Ca-dihydrate and Ca-phosphate are 0.91, 0.78, 0.8 and 0.76, respectively.

## DISCUSSION

To judge the benefit of gratings-based dark-field radiography for categorizing renal stones, one must consider the effect of the following observations. Half of the stones were mixed stones, the occurrence of the investigated stones varies between 10% and 79% and the X-ray attenuation and scattering signals contribute unevenly to the discernibility of the stone composition.

For example, the reason that the Ca-phosphate stones have the same R-value as the Ca-dihydrate stones may be due to the fact that they all contain Ca-dihydrate. Additionally, the uric acid stones absorb X-rays much less than the other stones which is the reason why they are discerned so well. Furthermore, the occurrence of the various calculi types plays an important role. The a priori statement that the stone type is Ca-monohydrate is true with a probability of 80%, whereas the probability that a stone contains predominantly Ca-phosphate is less than 50% even if the test by the R-value method was positive.

Scherer at al. reported nearly perfect identification of uric acid stones (AUC of 0.99 for the differentiation against oxalate and AUC of 0.95 for the differentiation against mixed stones) and a good identification of oxalate stones (AUC of 0.93 for the differentiation against mixed stones) [19]. We obtained a weaker identification capability but our study differs significantly. We investigated 322 stone fragments of 96 patients instead of 118 fragments obtained from 18 patients. Our sample cohort used for the ROC curves was the number of stone retrievals (104) and not the number of stone fragments which might be the reason why we have a larger proportion of mixed stones.

## CONCLUSIONS

The dark-field signal arises from the scattering of X-rays at microscopic interfaces due to refraction and, therefore, is not directly sensitive to the crystalline structure or the chemical composition. In the case of Uric acid stones, it is mainly their weak attenuation of X-rays which allows distinguishing them from the other stones. Therefore, gratings-based dark-field imaging is a non-destructive and potentially non-invasive technique that allows to discriminate between uric acid and non-uric acid stones in an experimental setup, which from a clinical point of view represents by far the most important question for stone treatment.

### CONFLICTS OF INTEREST

The authors declare no conflicts of interest.

## References

1. Stamatelou KK, Francis ME, Jones CA, Nyberg LM, Curhan GC. Time trends in reported prevalence of kidney stones in the United States: 1976-1994. Kidney Int. 2003; 63: 1817-1823.

2. Hesse A, Brändle E, Wilbert D, Köhrmann KU, Alken P. Study on the prevalence and incidence of urolithiasis in Germany comparing the years 1979 vs. 2000. Eur Urol. 2003; 44: 709-713.

3. Sánchez-Martín FM, Millán Rodríguez F, Esquena Fernández S, et al. Incidence and prevalence of published studies about urolithiasis in Spain. A review. Actas Urol Esp. 2007; 31: 511-520.

4. Yasui T, Okada A, Urabe Y, et al. A replication study for three nephrolithiasis loci at 5q35.3, 7p14.3 and 13q14.1 in the Japanese population. J Hum Genet. 2013; 58: 588-593.

5. Türk C, Neisius A, Petrik A, al. Urolithiasis. EAU Guidelines. Edn. presented at the EAU Annual Congress Amsterdam 2020. ISBN 978-94-92671-07-3. EAU Guidelines Office, Arnhem, The Netherlands. http://uroweb.org/guidelines/compilations-of-all-guidelines/

6. Tian D, Li N, Huang W, Zong H, Zhang Y. The efficacy and safety of adrenergic alpha-antagonists in treatment of distal ureteral stones in pediatric patients: A systematic review and meta-analysis. J Pediatr Surg. 2017; 52: 360-365.

7. Landau EH, Shenfeld OZ, Pode D, et al. Extracorporeal Shock Wave Lithotripsy in Prepubertal Children: 22-Year Experience at a Single Institution With a Single Lithotriptor. J Urol. 2009; 182: 1835-1840.

8. Türk C, Petřík A, Sarica K, et al. EAU Guidelines on Interventional Treatment for Urolithiasis. Eur Urol. 2016; 69: 475-482.

9. Kourambas J, Aslan P, Teh CL, Mathias BJ, Preminger GM. Role of Stone Analysis in Metabolic Evaluation and Medical Treatment of Nephrolithiasis. J Endourol. 2001; 15: 181-186.

10. Hesse A, Kruse R, Geilenkeuser WJ, Schmidt M. Quality control in urinary stone analysis: results of 44 ring trials (1980-2001). Clin Chem Lab Med. 2005; 43: 298-303.

11. Sutor DJ, Scheidt S. Identification standards for human urinary calculus components, using crystallographic methods. Br J Urol. 1968; 40: 22-28.

12. Michel T, Rieger J, Anton G, et al. On a dark-field signal generated by micrometer-sized calcifications in phase-contrast mammography. Phys Med Biol. 2013; 58: 2713-2732.

13. Schleede S, Meinel FG, Bech M, et al. Emphysema diagnosis using X-ray dark-field imaging at a laser-driven compact synchrotron light source. Proc Natl Acad Sci. 2012 ;109: 17880-17885.

14. Yashiro W, Terui Y, Kawabata K, Momose A. On the origin of visibility contrast in x-ray Talbot interferometry. Opt Express. 2010; 18: 16890.

15. Davis TJ, Gao D, Gureyev TE, Stevenson AW, Wilkins SW. Phase-contrast imaging of weakly absorbing materials using hard X-rays. Nature. 1995; 373: 595-598.

16. Wilkins SW, Gureyev TE, Gao D, Pogany A, Stevenson AW. Phase-contrast imaging using polychromatic hard X-rays. Nature. 1996; 384: 335-338.

17. Weitkamp T, Diaz A, David C, et al. X-ray phase imaging with a grating interferometer. Opt Express. 2005; 13: 6296.

18. Pfeiffer F, Weitkamp T, Bunk O, David C. Phase retrieval and differential phase-contrast imaging with low-brilliance X-ray sources. Nat Phys. 2006; 2: 258-261.

19. Scherer K, Braig E, Willer K, et al. Non-invasive Differentiation of Kidney Stone Types using X-ray Dark-Field Radiography. Sci Rep. 2015; 5: 9527.

20. Scherer K, Braig E, Willer K, Willner M, Fingerle AA, Chabior M et al. Non-invasive differentiation of kidney stone types using X-ray dark-field radiography. Sci Rep. 2015; 5: 9527.

21. Wang Z, Hauser N, Singer G, et al. Non-invasive classification of microcalcifications with phase-contrast X-ray mammography. Nat Commun. 2014; 5: 3797.

22. Wang Z, Hauser N, Singer G, et al. Correspondence: Reply to 'Quantitative evaluation of X-ray dark-field images for microcalcification analysis in mammography'. Nat Commun. 2016; 7: 10868.

23. Weitkamp T, Diaz A, David C, et al. X-ray phase imaging with a grating interferometer. Opt Express. 2005; 13: 6296.

24. Acharya S, Goyal A, Bhalla AS, et al. In vivo characterization of urinary calculi on dual-energy CT: going a step ahead with sub-differentiation of calcium stones. Acta Radiol. 2015; 56: 881-889.